Journal of Environmental Radioactivity 273 (2024) 107382

Contents lists available at ScienceDirect

Journal of Environmental Radioactivity

journal homepage: www.elsevier.com/locate/jenvrad

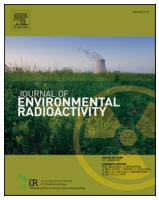

Upscaling ground-based backpack gamma-ray spectrometry to spatial resolution of UAV-based gamma-ray spectrometry for system validation

Sven Altfelder [a,*], Benedikt Preugschat [a,b], Milan Matos [c], Felix Kandzia [d], Benjamin Wiens [e], Otabek Eshmuradov [f], Christian Kunze [d]

[a] Federal Institute for Geosciences and Natural Resources (Bundesanstalt für Geowissenschaften und Rohstoffe, BGR), Stilleweg 2, D-30655, Hannover, Germany
[b] Leibniz University Hannover (LUH), Stilleweg 2, D-30655, Hannover, Germany
[c] International Atomic Energy Agency, Vienna International Centre, A-1220, Vienna, Austria
[d] IAF-Radioökologie GmbH, Wilhelm-Rönsch-Str. 9, D-01454, Radeberg, Germany
[e] Third Element Aviation GmbH, Brönninghauser Str. 38, D-33729, Bielefeld, Germany
[f] Radiation and Nuclear Safety Department of the Inspectorate on Control of Mining, Geological, and Industrial Safety, 27, A. Navoiy str, Tashkent, Uzbekistan

ARTICLE INFO

Keywords:
Airborne gamma-ray spectrometry (GRS)
Uncrewed aerial vehicle (UAV)
Uranium legacy sites
Upscaling
Variogram
Kriging

ABSTRACT

Advances in the development of gamma-ray spectrometers have resulted in devices that are ideal for use in conjunction with the increasingly reliable systems of autonomously flying uncrewed aerial vehicles (UAVs) that have recently become available on the market. Airborne gamma-ray spectrometry (GRS) measurements have many different applications. Here, the technique is applied to a former uranium mining and processing site, which is characterized by relatively low specific activities and, hence, low count rates, requiring relatively large detectors and correspondingly big size UAVs. The future acceptance of the use of such UAV-based GRS systems for radionuclide mapping depends on their ability to measure absolute specific activities of natural radionuclides such as U-238 in near-surface soil that are consistent with the results of established and proven ground-based systems. To determine absolute specific activities on the ground, the gamma radiation data from airborne detectors must be corrected for attenuation caused by the flight altitude above ground. In recent years, mathematical procedures for altitude correction have been developed, that are specifically tailored to the working range of several tens of meters typical for UAVs. However, very limited experimental validation of these theoretical approaches is available. A very large dataset consisting of about 3000 UAV-based and 19,000 backpack-based measurements was collected at a low-grade uranium ore dump in Yangiabad, Uzbekistan. We applied different geostatistical interpolation methods to compare the data from both survey techniques by upscaling backpack data to airborne data. Compared to backpack systems, UAV-based systems have lower spatial resolution, so measurements average over larger areal units (or in geostatistical terminology: "spatial support"). Taking into account the change in spatial support, we illustrate that (1) the UAV-based measurements show good agreement with the upscaled backpack measurements and that (2) UAV surveys provide good delineation of contrasts of the relatively smooth U-238 specific activity distribution typical for former uranium mining and processing sites. We are able to show that the resolution of UAV-based systems is sufficient to map extended uranium waste facilities.

1. Introduction

Ground-based gamma-ray spectrometry (GRS) surveys are an established method to map an area with high spatial resolution in the order of a few meters. However, their area-wide application is often not possible due to topographically difficult terrain (Kunze et al., 2022; van der Veeke, 2023). Manned aerial surveys, e.g., with helicopters, do not have this problem and are largely terrain-independent (IAEA, 2003). However, their disadvantages are high costs and complex safety regulations for aircraft, which prescribe a minimum flight altitude, usually ≥ 100 m above ground, so that helicopter-based surveys cannot achieve the high spatial resolution that land-based surveys offer.

This is an opportunity for UAVs. They operate at relatively low altitudes (10–20 m above ground) and collect radionuclide information

* Corresponding author.
E-mail address: sven.altfelder@bgr.de (S. Altfelder).

https://doi.org/10.1016/j.jenvrad.2024.107382
Received 14 September 2023; Received in revised form 5 January 2024; Accepted 12 January 2024
Available online 23 January 2024

with a spatial resolution comparable to that of ground-based surveys. In comparison with backpack-based systems, they take advantage of their ability to fly over otherwise inaccessible areas and areas that would be dangerous to humans because of the steepness of the terrain, the risk of landslides, or potentially harmful (e.g., radioactive) contamination (Ridikas et al., 2023; van der Veeke, 2023).

Combining gamma-ray spectrometers with a UAV seems straightforward. However, it poses some challenges regarding the magnitude of the specific activity of the ground and its importance for the selection of a suitable gamma ray detector. Because of the relatively small payload of many commercial UAV systems, the use of smaller detectors was the most common choice in recent years (MacFarlane et al., 2014; Martin et al., 2015; Pirttijärvi and Oy, 2016). Small detectors work well, especially for surface or point sources that generate high detector count rates, e.g., damaged sealed radioactive sources or high contamination of soil associated with nuclear accidents (MacFarlane et al., 2014; Martin et al., 2016). In this case, they provide a good overview of the spatial distribution of total counts but also allow spectrometric evaluations. They are also suitable for medium to low count rates when spectrometric analysis of the data is not planned and the total count rate provides sufficient information.

In contrast, small gamma-ray spectrometers have been regarded as of little or no use for mapping specific activities of naturally occurring radionuclides that are present in the ground at comparatively low activities. This is true for soil science applications (e.g., K-40 as a proxy for the potassium content of the soil), exploration of radioactive ore deposits, or mapping radioactive soil contamination at uranium mining and processing sites or industrial sites with naturally occurring radioactive materials (NORM). Here, the overall count rates are usually much lower and the mapping targets are generally extended volume sources without distinct hot spots.

Therefore, it is a welcome development that in the field of commercial heavy-lift UAV with takeoff masses (MTOM) up to 25 kg, technological progress has been tremendous in recent years. The 25 kg limit is a defined boundary in European Union legislation (EU, 2019a; EU, 2019b) for operating a UAV in the category “open”. Using a UAV in the open category makes the planning and the execution of UAV operations easier. With payloads of up to 10 kg, a window has opened for the use of medium heavy gamma-ray spectrometers.

As part of the research project DUB-GEM a heavy-lift UAV with a of 25 kg and a detector payload of 8 kg was used to map the distribution of U-238 on a low-grade ore stockpile at a former uranium mining and processing site in Yangiabad, Uzbekistan. DUB-GEM stands for “Development of a UAV-based Gamma Spectrometry for the Exploration and Monitoring of Uranium Mining Legacies”. The UAV was designed and manufactured within the framework of the project and the flight surveys in Uzbekistan discussed here were part of a second measurement campaign in Central Asia within the project.

During postprocessing of airborne UAV data, in order to convert gamma-ray raw spectral data recorded at a certain altitude into absolute specific activities in the ground, analytical methods have to be applied. The necessary steps include footprint and height related corrections that take into account the attenuation of the gamma rays by the air layer between the ground and the detector and the height-dependent field of view (footprint) of the detector.

Height corrections are usually made using analytical models under the assumption that the soil is a semi-infinite homogeneous volume with uniform density and uniform radionuclide content. Duval et al. (1971) and Grasty et al., 1979, who focused on conventional airborne gamma-ray spectrometry using airplanes or helicopters, published early analytical models for the 50–250 m altitude range. Comprehensive guidelines for processing gamma-ray spectra using counts collected in energy windows around prominent photo-peaks of naturally occurring radionuclides, including approximate values for flight altitude corrections applicable to the conventional airborne operating range, are available in Nicolet and Erdi-Krausz (2003).

A common calibration procedure for conventional airborne GRS is to convert the corrected window count rates to specific activities of radionuclides on the ground by dividing them by a "sensitivity coefficient". Sensitivity coefficients are obtained by dividing the window count rates at the nominal measurement height by the corresponding average specific activity, determined from samples on the ground in a predetermined series of sections that are topographically flat with uniform radioactivity covering a range of radiometric signatures (IAEA, 2003). The spatial averaging of the ground data, usually collected with backpack measurements or soil sampling, over the footprint of the airborne GRS is usually done arithmetic under the assumption that the sections are homogeneous in terms of density and radionuclide content. The calibrated conventional airborne GRS is then used for the mapping of unknown areas. It is recommended to fully recalibrate airborne GRS calibrated every twelve months (Grasty and Minty, 1995).

For the natural radiation background, comparisons (ground truthing) of conventionally calibrated airborne helicopter GRS with ground-based measurements are rare (Kock and Samuelsson, 2011). By using single point comparisons, some authors ignore that the footprints of the two methods are quite different (Ogunsanwo et al. (2019) and Youssef (2016)). Others try to compensate for the differences in footprints by arithmetically averaging the ground-based data within the assumed footprints of the airborne measurements (Ammar, 1996; Bollhöfer et al., 2007, 2014). Acknowledging that the distance of a source to the detector plays a role, Kock and Samuelsson (2011) averaged the results of ground-based measurements within calculated, height-dependent footprints with an inverse distance weighting scheme before comparing airborne and ground-based data. The weights were calculated from the horizontal distance between the geolocation of the airborne measurement and the geolocation of the sample point on the ground. In another comparison, albeit for Cs-137, Tyler (1994) explicitly accounts for the fact that the spatial response of an airborne detector is centre-weighted by incorporating the detector response characteristic, and hence the quadratic dependence of source distance, into a weighing scheme of samples collected in a hexagonal sampling plan within the footprint.

Since applicability of the guidelines of Nicolet and Erdi-Krausz (2003) is limited to the conventional airborne operational range, van der Veeke et al. (2021a) developed altitude corrections for the UAV operational range of up to 40 m by extending the analytical models of Duval et al. (1971) and Grasty et al. (1979). In their approach, they do not have to resort to calculating a "sensitivity coefficient" to convert the count rates into specific activities of radionuclides on the ground. Instead, the calculation of specific activity is based solely on a physical model. The analytical approximation by van der Veeke et al. (2021a), validated by Monte Carlo simulations, shows that the attenuation of gamma radiation as a function of measurement height reduces the intensity at 40 m by 50% for the 1.46 MeV gamma of K-40. The Monte Carlo simulations allowed van der Veeke et al. (2021a) to also provide standard spectra that extend the applicability of altitude corrections from the window method to full spectrum analysis (see IAEA (2003) for a detailed explanation of these spectrometric methods).

Fully independent comparisons of absolute specific activities of radionuclides obtained from altitude-corrected airborne gamma-ray data with experimental data measured on the ground are even rarer than ground truthing of conventionally calibrated airborne systems as described above. Such a fully independent validation of specific activities calculated from UAV-borne GRS data, with measured ground-based data is described in van der Veeke et al. (2021a). Van der Veeke et al. (2021a) and co-workers compared altitude-corrected UAV measured specific activities for nuclides of the Th-232 series and K-40 measured at 13–35 m above a single geolocation in an agricultural field with field data mapped by a vehicle-based spectrometer. Count rates at different heights were then compared to the arithmetic average of measurements within a radius of 25 m around the geolocation used for validation. The comparison showed that the arithmetic mean of the specific activity measured on the ground falls within the $\pm 1\sigma$ band of the

altitude-corrected specific activities measured with the UAV.

On the same agricultural field (400 m by 800 m), van der Veeke et al. (2021b) compared Th-232 concentrations measured with airborne-UAV (at 20 m) and ground-based Th-232 measurements by ordinary block kriging (Burrough et al., 2015) of both data sets to same set of blocks dividing the field into 512 squares of size of 25 × 25 m^2. According to van der Veeke et al. (2021b) this block size was chosen to be equal to the line spacing of both surveys to make sure that each block contains measured data, while the possible consequences of the scaling properties of block kriging in interpolation are not discussed further, nor is this interesting property explicitly set in value for the comparison. This comparison showed an overestimation of 12–16% of the concentration measured by the UAV at 20 m compared to the concentration measured on the ground.

The GRS calibration/validation procedures described above have in common that most of them disregard the need for a distance-weighted averaging (which is a physical necessity in case of a spatially varying specific activity within the footprint). It is physically clear that radiation sources in the outer part of the footprint of an airborne system contribute less to the detector's count rate than areas directly under the detector in its center (Minty, 1997).

A distance-weighted averaging procedure, incorporating the height-dependent footprint, is a form of upscaling. In spatial statistics, upscaling is understood as the determination of average values over spatial supports larger than the sampling support of measurements (Neuweiler and Vogel, 2007), including situations where the attribute in question does not average arithmetically in space (Goovaerts, 1999). Non-arithmetic upscaling can be used to account for the physical necessity that different areas within the footprint contribute differently to the detector signal.

As indicated in the previous excursus, the spatially representative measurement of natural radionuclides in soils in the environment is a challenge due to their inherently heterogeneous distribution. This problem is exacerbated when attempting to relate spatially point scale soil measurements to non-point remote sensing observations. This work addresses this problem by investigating the relationship between the specific activity of U-238 measured with the well-established method of in situ backpack GRS and the emerging technology of UAV-based GRS over a spatially varying U-238 activity distribution on a low-grade ore dump in Yangiabad, Uzbekistan.

By applying geostatistical techniques to interpolate and upscale pointscale measured specific U-238 activities to different types of spatial support (squares, circles) representing the footprint of a UAV, we demonstrate how to approach the validation of a data set of UAV-borne GRS U-238 data with a data set measured with two backpack GRS systems across scale differences. The approach also includes the explicit consideration of the distance-dependent quantitative attenuation of the locally variable gamma ray emissions within the UAV's footprint on the measured cumulative detector signal of the UAV.

2. Materials & methods

2.1. Study area

The Y7 low-grade ore heap is located south of Yangiabad, Uzbekistan on the right bank of the Dukentsay River and consists of very coarse material (with grain diameters: 20 … 500 mm). It is part of an ensemble of waste rock and ore sorting waste disposed of near the uranium deposits around the town of Yangiabad, north of the town of Angren, where several economically mineable uranium deposits were discovered in the 1950s. At the site of Y7, low-grade ore was stored in a large dump in a side valley of the Dukentsay River presumably with the intention to process it at a later stage during the life of the mine, but actually was never processed and is therefore still there. Operations at the Yangiabad mines and concentration plant ceased in the 1980s, leaving all associated sites without environmental remediation. Y7 is characterised by a large plateau with ripples of 0.5–1 m depth and spacing of approximately 5 m. Its slopes are steep with a slope angle of more than 40° that are close to the natural angle of repose and are not vegetated. There is only sparse vegetation on the plateaus with species adapted to dry conditions.

2.2. Equipment

A detailed description of the equipment previously used in a previous measurement campaign in Kyrgyzstan and Kazakhstan (flights were carried out in both countries in 2021) including the UAV and the gamma ray spectrometers used can be found in Kunze et al. (2022) and Preugschat et al. (2022).

2.2.1. Gamma ray spectrometers used in backpack surveys

The backpack surveys were carried out using a Medusa MS-1000 NaI (Tl) scintillation detector with silicon photo multiplier (called Medusa-A in the following) and a Nuvia PGIS-2 NaI(Tl) scintillation detector (called Nuvia in the following) with a photo multiplier tube (PMT). For detailed specifications see Table 1. Measurements were made with the Nuvia detector on the low-grade Y7-ore stockpile on four different days (August 11, 12, 13, and 15, 2022). 16501 data points were collected. The Medusa detector was used to measure on the Y7 site on two different days (on August 14 and 15, 2022). 7816 data points were collected. The recording interval was 1 Hz with both detectors.

The number of decimal places in the recording of geographic coordinates is limited to 6 digits for the Nuvia detector. Therefore, the uncertainty of the recording in the latitude range of Yangiabad is about 10 cm. This leads to duplications in the coordinates of the second-by-second backpack measurements, since it depends on the actual walking speed (which may vary depending on the terrain and the need for breaks) whether the GPS coordinate changes within this uncertainty range or not. To avoid potential bias from averaging coordinate duplicates, we instead removed duplicates, leaving 10855 data points in the Nuvia dataset for further data analysis.

2.2.2. UAV-based gamma spectrometer

The UAV detector system considered here, developed in the DUBGEM project (hereafter referred to as Medusa-B), is a CeBr3 scintillation detector manufactured by Medusa Radiometrics Ltd (Netherlands). For detailed specifications see Table 1. The height above the ground for the UAV measurements is 10 m at a ground speed of approximately 3 m/s (twice as fast as the backpack walks). UAV-based measurements were made on the low-grade Y7-ore stockpile on 2 different days (August 13 and 15, 2022). 2840 data points were collected (1 Hz recording interval) during four separate surveys.

2.2.3. Data processing

The choice of a large crystal in the UAV-based gamma spectrometer derived from many years of experience in airborne helicopter GRS. For natural background radiation and especially uranium legacy sites, it provides sufficiently high counting rates and thus a satisfactory counting statistics within the time step of data acquisition (1 Hz). This is especially advantageous for large, laterally dispersed sources with low specific activity or high ground speed. The time period for averaging the

Table 1
Detector systems used.

	NaI (Medusa-B)	NaI (Nuvia)	CeBr3 (Medusa-A)
Crystal dimensions (inches)	3 x 9	4 x 4 x 8	3 x 6
Crystal volume (ml)	1000	2000	700
FWHM at 662 keV (%)	8.5	8.5	<3.9
Number of spectral channels	512	256	2048[a]

[a] Alternative configurations with 300, 512, 1024 channels may be selected.

count rates may be varied in the spectrum evaluation procedure. The relevant, detectable gamma emitters are Bi-214/Pb-214 for the U-238 series. Within this paper we use the term U-238 for the uranium series. Calculation of specific activities for U-238 assumes equilibrium of the decay chain. For both Medusa detectors, Full Spectrum Analysis (IAEA, 2003) is used to extract radionuclide concentrations from the measured spectra. For the Nuvia detector, the window method (IAEA, 2003) is used. The UAV-borne measurements with the Medusa-B detector have been analysed by using the protocol and the spectral height corrections described in van der Veeke et al. (2021a).

3. Theory

When trying to estimate the value of a variable z at unsampled locations in a domain with known sample data $z(x_1), z(x_2), \cdots, z(x_n)$ on a given support at locations $x_1, x_2, \cdots, x_n$, a spatial interpolation technique has to be applied. A brief overview of the different kriging interpolation techniques used in this study is given here.

3.1. Ordinary kriging

The value of z_{OK} at an unsampled location x_0 on the same support is computed by

$$z_{OK}(x_0) = \sum_{i=1}^{N} \omega_i z(x_i) \tag{1}$$

Here N is the actual number of neighboring observations chosen for the estimation of z_{OK}, ω_i are the weights assigned to each observation. For calculating ω_i an auxiliary function including the error variance at the unsampled location,

$$f(\omega_i, \lambda(x_0)) = Var(z_{OK}(x_0) - z(x_0)) - 2\lambda(x_0)\left(\sum_{i}^{N} \omega_i - 1\right) \tag{2}$$

Is minimized with regard to ω_i and the Lagrange multiplier $\lambda(x_0)$ by calculating its partial derivatives where $z(x_0)$ is the actual (unknown) value at location x_0. Doing so, a system of linear equations is obtained,

$$\sum_{i=1}^{N} \omega_i \gamma(x_i, x_j) + \lambda(x_0) = \gamma(x_i, x_0) \quad for\ j = 1, 2, \cdots, N \tag{3}$$

$$\sum_{i=1}^{N} \omega_i = 1 \tag{4}$$

Solving (3) with condition (4) provides the N weights ω_i needed to solve equation (1). $\gamma(x_i, x_j)$ is the semivariance for the respective lag h including x_i and x_j. It is obtained from a semivariogram model fitted to experimental semivariances

$$\gamma^*(h) = \frac{1}{2M(h)} \sum_{i=1}^{M(h)} [z(x_i) - z(x_i - h)]^2 \tag{5}$$

With $M(h)$ being the number of data pairs for a given distance h. For an in-depth introduction to the concept of kriging see Webster and Oliver (2001).

3.2. Ordinary block kriging

Depending on the application, it may be of importance to estimate the value of z on a different support such as a block B of a certain area. The ordinary kriging estimate $z_{OK}(B)$ for a block is still a weighted sum of the surrounding data,

$$z_{OK}(B) = \sum_{i=1}^{N} \omega_i z(x_i) \tag{6}$$

However, the kriging system to be solved changes to

$$\sum_{i=1}^{N} \omega_i \gamma(x_i, x_j) + \lambda(x_0) = \overline{\gamma}(x_i, B) \quad for\ j = 1, 2, \cdots, N \tag{7}$$

$$\sum_{i=1}^{N} \omega_i = 1 \tag{8}$$

With $\overline{\gamma}(x_i, B)$ being the point to block semivariance.

3.3. Non-arithmetic krige averaging

In UAV-based GRS, the concentration distribution of the gamma-emitting radionuclides within the assumed footprint of a detector does not contribute uniformly to the overall signal of the detector due to the distance-dependent attenuation of the gamma signal. This is not taken into account by the arithmetic averaging process that is inherent to ordinary block kriging.

To account for this non-uniform contribution, we assume a circular footprint centered at the position (x,y) of the detector mounted on the UAV and having a certain radius representing the field of view. Using ordinary kriging with data measured at point scale we estimate n point estimates $z(x_i, y_i)$ of the specific activity on a uniform grid within this footprint (schematically shown in Fig. 1). In subsequent step, weighted averages are calculated from these n point estimates. Weights are derived from the distance dependent calculation formula for the radionuclide dependent count signal $S_D(x, y)$ of a UAV-mounted detector at location (x, y), the value of which is proportional to the corresponding estimate of the UAV measured specific activity $DC_{U-238}(x, y)$:

$$S_D(x, y) = \int_0^{\infty} \int_0^{2\pi} d\varphi r\, dr\, \frac{1}{r^2 + h_D{}^2}\ e^{-\sqrt{r^2 + h_D{}^2}\mu_a \rho_a} c(r, \varphi)\ \alpha_D \tag{9}$$

Here α_D is the efficiency of the detector, ρ_a is the density of air, μ_a is the mass attenuation coefficient (at 1.77 MeV, U-238 Series), r is the radial distance to the geolocation of the UAV, h_D is the height of the UAV above ground (here 10 m) and $c(r, \varphi)$ is the spatially varying specific activity of the ground.

The distance-weighted average of the kriged n point estimate $z(x_i, y_i)$ is calculated by:

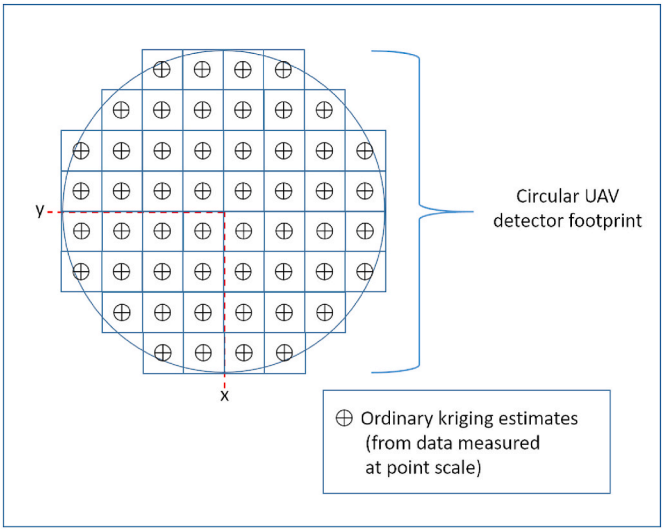

Fig. 1. Schematic representation of the circular UAV footprint centered on the geodetic location (x,y) of a UAV measurement with n ordinary kriging estimates (from data measured at point scale) on a regular grid within the footprint.

$$C_{U-238}(x,y)=\frac{\sum_{i=1}^{n}\frac{1}{r_i^2+h_D^2}\ e^{-\sqrt{r_i^2+h_D^2}\mu_a\rho_a}\ z(x_i,y_i)}{\sum_{i=1}^{n} r_i^2+h_D^2\Big/e^{-\sqrt{r_i^2+h_D^2}\mu_a\rho_a}} \quad (10)$$

$C_{U-238}(x,y)$ is an estimate for $DC_{U-238}(x,y)$, assuming that the UAV detector signal is corrected with the procedure described in van der Veeke et al. (2021a) to the height of backpack measurements (1 m) and α_D is accounted for in the conversion of $S_D(x,y)$ to $DC_{U-238}(x,y)$.

3.4. Validation criteria

Correlation between the various observed and predicted specific U-238 activities was assessed using the Pearson correlation coefficient

$$r=\frac{\sum_{i=1}^{n}(z_{Obs}(x_i)\ -\ \bar{z}_{Obs})(\ z_{OK}(x_i)-\bar{z}_{OK})}{\sqrt{\sum_{i=1}^{n}(z_{Obs}(x_i)\ -\ \bar{z}_{Obs})^2}\sqrt{\sum_{i=1}^{n}(z_{OK}(x_i)-\bar{z}_{OK})^2}} \quad (11)$$

where $z_{Obs}(x_i)=[z_{Obs}(x_1)\cdots z_{Obs}(x_n)]$ is the data set array (measured data) and $z_{OK}(x_i)=[z_{OK}(x_1)\cdots z_{OK}(x_n)]$ is the estimation using different kriging approaches.

4. Comparison and merging of the two sets of GRS data measured with different backpack detectors

Since two different detectors (Medusa-A and Nuvia) were used for ground-based GRS, it was investigated whether the characteristics of the two data sets are compatible and allow merging into one data set.

Fig. 2 shows the routes followed during backpack measurements with the Nuvia (red) and Medusa-A (blue) detectors on Y7. The height above the ground for the backpack measurements is 1 m. Note that the area covered by the Medusa-A detector is smaller than the area covered by the Nuvia detector.

Table 2 shows the summary statistics of the specific activities for U-238 measured with both detectors. The shape of both distributions is similar, as seen especially in the 1st and 3rd quartiles, median and mean. Both distributions are positively skewed, but at the edge of being considered approximately symmetric (skewness between −0.5 and 0.5). The kurtosis values lower than, but close to 3 indicate that both distributions have a slight negative excess kurtosis compared to a normal distribution. Based on their approximate normal character we abstained from transforming data.

Before we decided to merge both datasets, we examined their spatial statistics. For this, we first performed a) a variogram analysis of the two individual datasets and b) a variogram analysis of the merged dataset.

Table 2
Summary statistics for the specific activities of U-238 measured at the heap of low-grade ore, Y7 with the Medusa-A and the Nuvia backpack detectors.

Heap Y7	MEDUSA-A U-238 (Bq/kg)	NUVIA U-238 (Bq/kg)	Specific activity ratio MEDUSA-A/NUVIA
Min.	72.88	68.36	1,07
1st Qu.	521.51	502.77	1,04
Median	900.91	925.55	0,97
Mean	966.06	967.16	1,00
3rd Qu.	1371.41	1354.38	1,01
Max.	2856.01	3326.74	0,86
Standard deviation	525.09	542.00	–
Coefficient of variation [%]	54	56	–
Skewness	.50	.53	–
Kurtosis	2.52	2.93	–

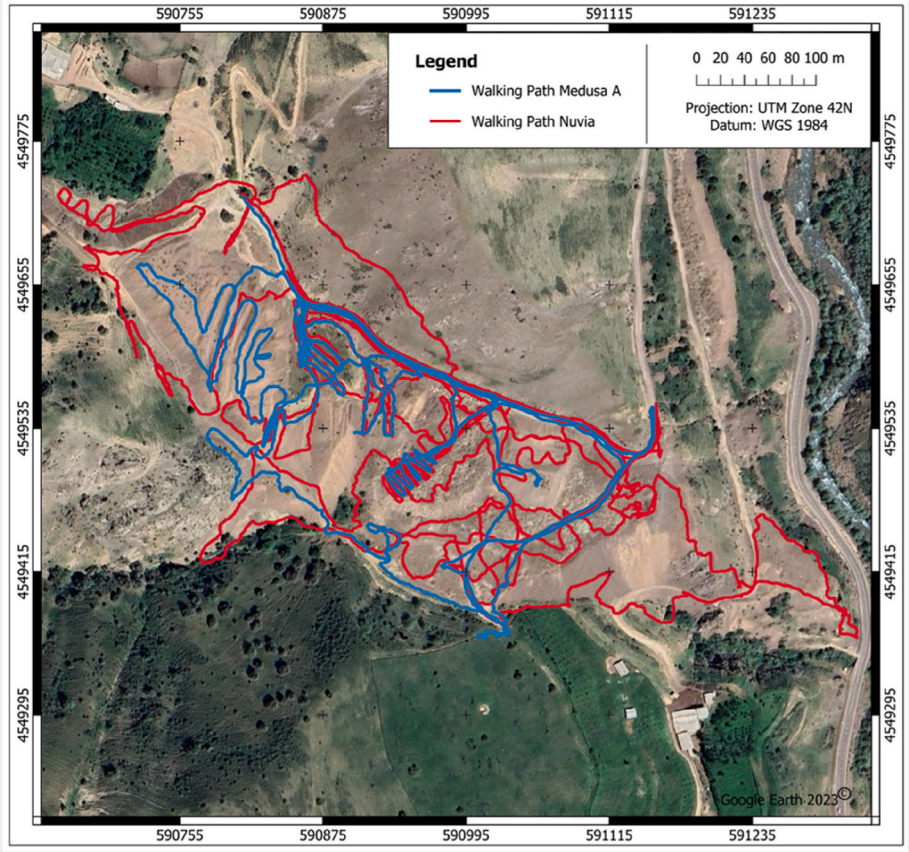

Fig. 2. Location of the tracks followed during backpack measurements with the Nuvia (red) and Medusa-A (blue) detectors on the low-grade Y7 ore stockpile. (For interpretation of the references to color in this figure legend, the reader is referred to the Web version of this article.)

We investigated spatial anisotropy by calculating directional semivariograms, but no relevant zonal or geometric anisotropy was detected. During mining, the material from the low-grade ore heap studied here passed through a sorting mechanism that sorted the material so that its specific activity was within a range of predetermined thresholds. Below the lower threshold, the material was disposed of as waste; above the upper threshold, the material was immediately processed for uranium recovery. This explains the narrow range of U-238 activities observed and, as the material was well mixed during transport and sorting, the lack of trend or zonation.

Fig. 3 shows the spatial continuity of the three datasets based on their respective omnidirectional semivariograms. Estimation of semivariances was carried out using a lag distance of 1 m and a cutoff of 150 m. Based on the large amount of data gathered with both detectors, semivariances are stable despite this rather small lag distance. The visual comparison of the three semivariograms shows a similar progression over distance. Variogram functions were fitted to data using the programming language R (R Core Team, 2021) package *gstat* (Pebesma et al. (2015)) where variogram parameters for a set of models (Spherical, Matern, Exponential) are fitted to the sample variogram and the best fitting model is returned (Pebesma, 2004). Residuals in least square estimation were weighted by $\frac{n(h)}{h^2}$ with $n(h)$ the number of point pairs and h the distance. Supported by practice, this is the default method in *gstat*.

For all three sample variograms, the best fitting model is the exponential model. Nugget variance c_0, partial sill c (sill minus the nugget) and range r of the exponential model fitted to the sample variograms are given in Table 3. All model parameters are quite similar. The nugget variance is rather small with a relative nugget effect ranging from 0 to 2 % of sill. The range parameter varies from 33 to 56 m.

As a further plausibility check whether both data sets are suitable for merging, kriging cross validation was applied. In the approach we separated estimation of the sample variogram and the variogram function completely from model validation. The variogram function used for kriging was the one exclusively estimated on the Nuvia data (Table 3 and middle panel of Fig. 3). The data set used for validation is the one exclusively measured with the Medusa-A detector. This choice stems from the fact that the survey area covered by the Nuvia detector includes the smaller survey area covered by the Medusa-A detector (see Fig. 2). This guarantees that there are sufficient data points within semivariogram range around the Medusa-A measurement locations. Beyond range prediction is avoided. Conversely, this is not the case as many Nuvia measurements are located beyond semivariogram range from the Medusa-A data. In Fig. 4 the corresponding scatter plot of observed vs. kriged predicted U-238 specific activity estimates at the Medusa-A measurement locations on Y7 is shown. Fitting a linear model ($y = ax$) to the data set of Fig. 4 leads to an estimated slope of approximately one (1.014), indicating that there is no detector-dependent measurement bias. The r of 0.88 indicates a good correlation between the specific activities of U-238 observed with Medusa-A and the corresponding linear model fitted to the krige predictions based on the Nuvia data.

Mean and standard deviation of the estimations are shown in Table 4. Both agree well with the respective observed Medusa-A values shown in Table 2. This indicates that the smoothing effect (loss of variance) inherent in kriging is very small to non-existent (Oliver and Webster, 2014). Since smoothing increases with increasing nugget-sill ratio, it does not play a significant role in the present case, since there is practically no nugget effect. The sample variance is therefore largely preserved in the interpolation.

The previous analysis provides good insight into the correspondence between the spatial statistics of the two datasets, and the results support the decision to merge both datasets into one.

5. Comparison of backpack data with UAV-based GRS survey

The UAV-based GRS survey was carried out with a third detector

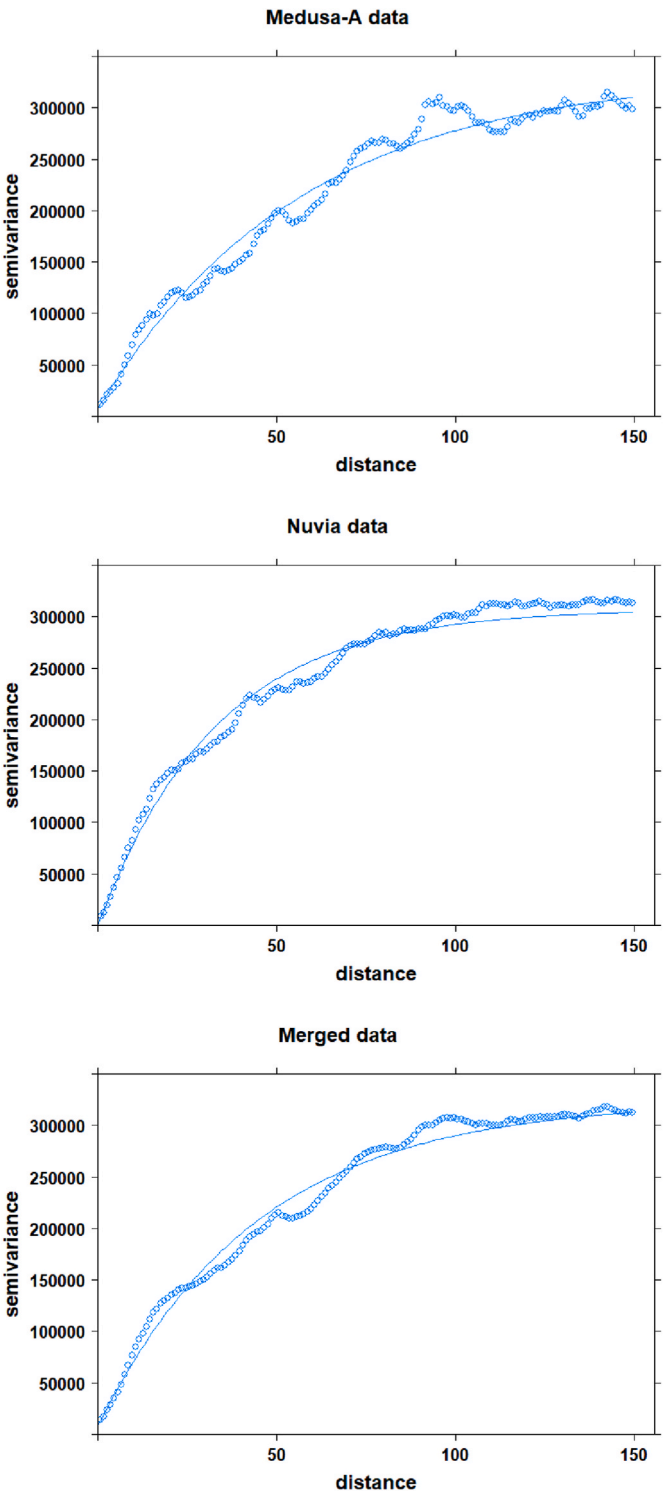

Fig. 3. Omnidirectional semivariograms for the Medusa-A, Nuvia and merged data from Y7.

Table 3
Nugget variance, sill and range of the exponential model.

Data	Nugget	Sill	Range(m)
Medusa-A	*7493*	*325965*	*56*
Nuvia	*0*	*307839*	*33*
Merged	*7954*	*316008*	*45*

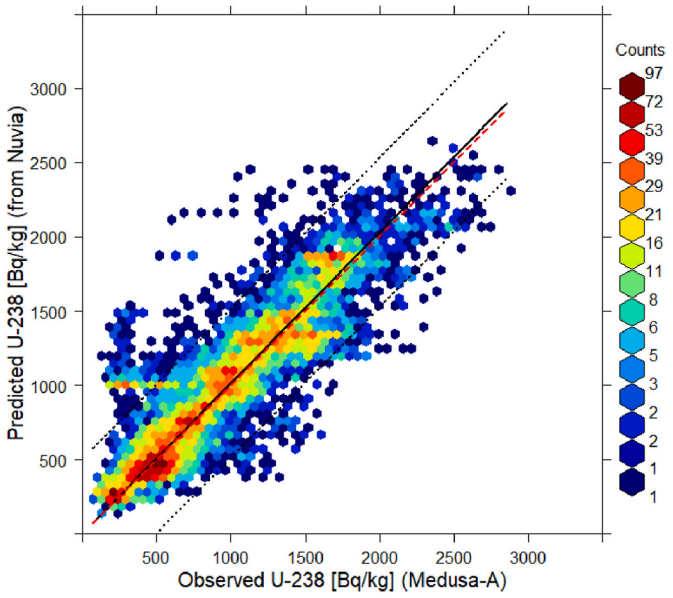

Fig. 4. Scatter plot of observed vs. kriged predicted Medusa-A backpack specific activities of U-238. Variogram estimation and ordinary kriging interpolation was done with Nuvia data. Note that the data is binned in hexagonal bins. The color represents the number of data points within each bin. The dashed red line is the 1:1 line. The solid black line is the linear regression line forced through zero. The dashed black lines indicate the 95 % prediction band. (For interpretation of the references to color in this figure legend, the reader is referred to the Web version of this article.)

Table 4
Number of predictions n, mean m, standard deviation σ and standardized cross validation statistics of the kriged estimates.

	Predicted Medusa-A data
n	*7816*
m	*1023*
σ	*513*

(Medusa-B). Fig. 5 shows the trajectories of the UAV during the surveys.

Table 5 shows the summary statistics of the specific activities for U-238 measured with the Medusa-B detectors after correcting data from 10 m to ground height taking into account the attenuation of the gamma rays due to the layer of air between the ground and the detector. The following comparison with the summary statistics of the backpack surveys (Table 2) reveals a higher mean (Factor 1.58) and a lower coefficient of variation (25% versus 55%). With a skewness of 0.1, the distribution is approximately symmetrical. The slight negative excess kurtosis is very similar to the backpack data.

The lower coefficient of variation shows that there is a smoothing effect when collecting data at 10 m height due to the spatial averaging of the specific activities, as the field of view (footprint) of the detector increases. According to van der Veeke et al. (2021a), for a UAV-based GRS survey at 10 m, the recommended range for the selection of the detector footprint radius is 22–91 m, corresponding to 65–95% of the measured radiation based on the model assumption of a semi-infinite homogeneous volume.

The Matern model best fits the sample variogram estimated from the Medusa-B data (lag distance 1 m and cutoff 115 m) shown in Fig. 6. The nugget variance is 2 % of sill, the range is 42 m and kappa is 1 (Table 6). The fact that the best fitting variogram model is the Matern model with a kappa value of 1 is an additional indicator for the smoothing effect mentioned above. Nugget and range parameter of the model are comparable to the estimates in Table 3. The main difference is in the sill, which is only 75 % of the sill of the exponential model of the merged backpack data set shown in Table 3, confirming the smoothing effect of measuring specific activities of U-238 with a UAV at greater height. The summary statistics a well as the variogram model show obvious differences in spatial support (footprint) between UAV and backpack data - even after correcting the UAV data to account for the height dependent signal attenuation.

The simplest approach to compare the height-corrected UAV-measured specific activities with the ground-based measured specific activities is ordinary kriging cross-validation using the merged backpack point data (Fig. 2) and the variogram function estimated from this data (Table 3 and bottom panel of Fig. 3). Cross-validation is performed by comparing the UAV-measured specific activities with the kriged point estimates at the geodetic locations of the 2840 UAV measurements.

In a second approach we accounted for the fact that the specific activities measured with the UAV was measured on a different support (footprint). Estimation was done by ordinary block kriging. Block averages are obtained by kriging point data to rectangular blocks of predefined size, centered in this case on the geodetic coordinates of the UAV measurements. To approximate the detector footprint of the UAV, which corresponds to 65% of the measured radiation (van der Veeke et al., 2021a), a square block with an area corresponding to a circle with a radius of 22 m (side length of the square block: 39 m) is chosen for interpolation and the successive ordinary block kriging cross-validation.

In a third and final approach, we account for the fact that the detection process on a UAV is better approximated by a non-arithmetic spatial aggregation of data at point support (point estimates) within a circular footprint. In this way, we take into consideration the fact that the quantitative impact of local gamma emissions on the cumulative UAV detector signal is distance dependent and corresponds to the position of its corresponding local emission source at point support relative to the position of the UAV above a circular detector footprint. Using the non-arithmetic Krige averaging approach described in section 3.3, we assumed circular footprints with 22 m radius (65% of the UAV detector signal at height 10 m according to van der Veeke (2023)) centered on the 2840 geodetic locations of the UAV measurements. In a second step we used the merged backpack data to estimate n ($n \approx 56$) point estimates $z(x_i, y_i)$ of the specific activity of U-238 on a uniform grid (cell size 5.2 m) within each circular footprint In subsequent step, using equation (10), weighted, non-arithmetic averages were calculated from the n point estimates within each circular footprint.

Fig. 7 shows the corresponding scatter plots of observed versus predicted specific activities of U-238 as estimated with the three different kriging approaches described above. Fitting a linear model ($y = ax$) to the three datasets shown in Fig. 7 results in an estimated slope of 0.78 in all three cases. Systematic underestimation (bias) of the UAV-observed specific activity of about 22 % is independent of the chosen interpolation method. From top to bottom panel in Fig. 7 the correlation coefficent r is 0.83, 0.89 and 0.89. From the increase in r, it can be seen that the predictive power of the kriging model increases when the change in support is accounted for by block kriging or non-arithmetic krige averaging.

The results of block kriging and non-arithmetic krige averaging are quite similar when comparing the middle and bottom panels of Fig. 7. The distance dependence of the detector signal seems to have only a small influence on the UAV reading. One reason for this could be that the site Y7 is a fairly well sorted, low grade ore stockpile where the specific activity of U-238 does not show particularly pronounced activity contrasts as the material has passed through sorting. Distance dependence of the recorded detector signal will be most noticeable if the activity contrasts of the object being mapped are very pronounced. However, a closer look at the lower panel of Fig. 7 shows that the specific activities near the maximum of the data range in particular seem to be better approximated indicating that hotspots are better represented by the weighted non-arithmetic averaging process.

Assuming that the distribution of specific activities of U-238 on the

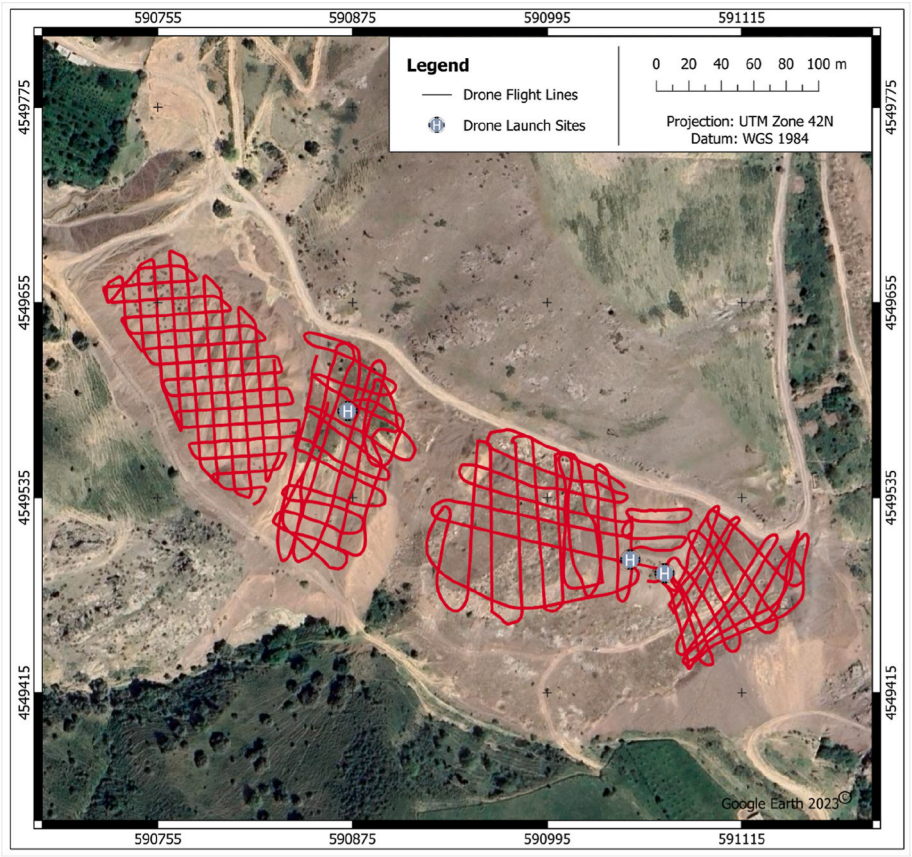

Fig. 5. Flightlines of the UAV mounted Medusa-B detector on the low-grade Y7 ore stockpile. (For interpretation of the references to color in this figure legend, the reader is referred to the Web version of this article.)

Table 5
Summary statistics for the specific activities of U-238 measured at the heap of low-grade ore, Y7 with the Medusa-B UAV-based detector.

Heap Y7	MEDUSA-B *U-238 (Bq/kg)*
Min.	582.9
1st Qu.	1255.5
Median	1497.3
Mean	1528.3
3rd Qu.	1823.1
Max.	2913.3
Standard deviation	382.9
Coefficient of variation [%]	25
Skewness	.092
Kurtosis	2.51

site Y7 can be modelled as a random process with spatial autocorrelation, kriging provides the best linear unbiased prediction at unsampled locations (Matheron, 1963). In our earlier analysis of the two backpack data sets, we convincingly showed that the evidence for this assumption is strong.

A possible explanation for the observed bias is the effect of shielding by the operator's body during backpack measurements. The 22% underestimation observed here is in the range of the ~15 % attenuation of higher energy gamma rays from natural sources found by Buchanan et al. (2016) for measurements with a backpack system worn at about 1 m above ground. A similar shielding effect was also postulated by van der Veeke et al. (2021b) who observed a 12–16 % overestimation when comparing UAV airborne data measured at an altitude of 20 m with tractor measurements assuming a small shielding effect due to the tires of the vehicle.

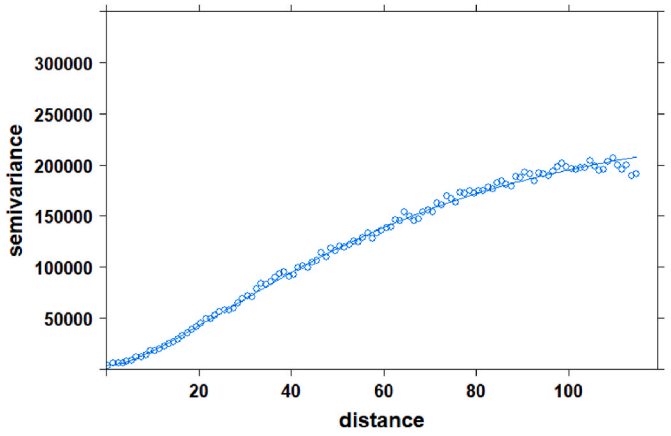

Fig. 6. Omnidirectional semivariogram for the UAV-based Medusa-B data from Y7.

Table 6
Nugget variance, sill and range of the Matern model for the UAV-based Medusa-B data.

Data	Nugget	Sill	Range(m)	Kappa
Medusa-B	3680	240175	42	1

Another explanation could be that a systematic overestimation of 22 % occurred during data processing and/or during the height correction from 10 m of the Medusa-B data. For further considerations, we operationally reduce the Medusa-B data by 22%, knowing full well, that the

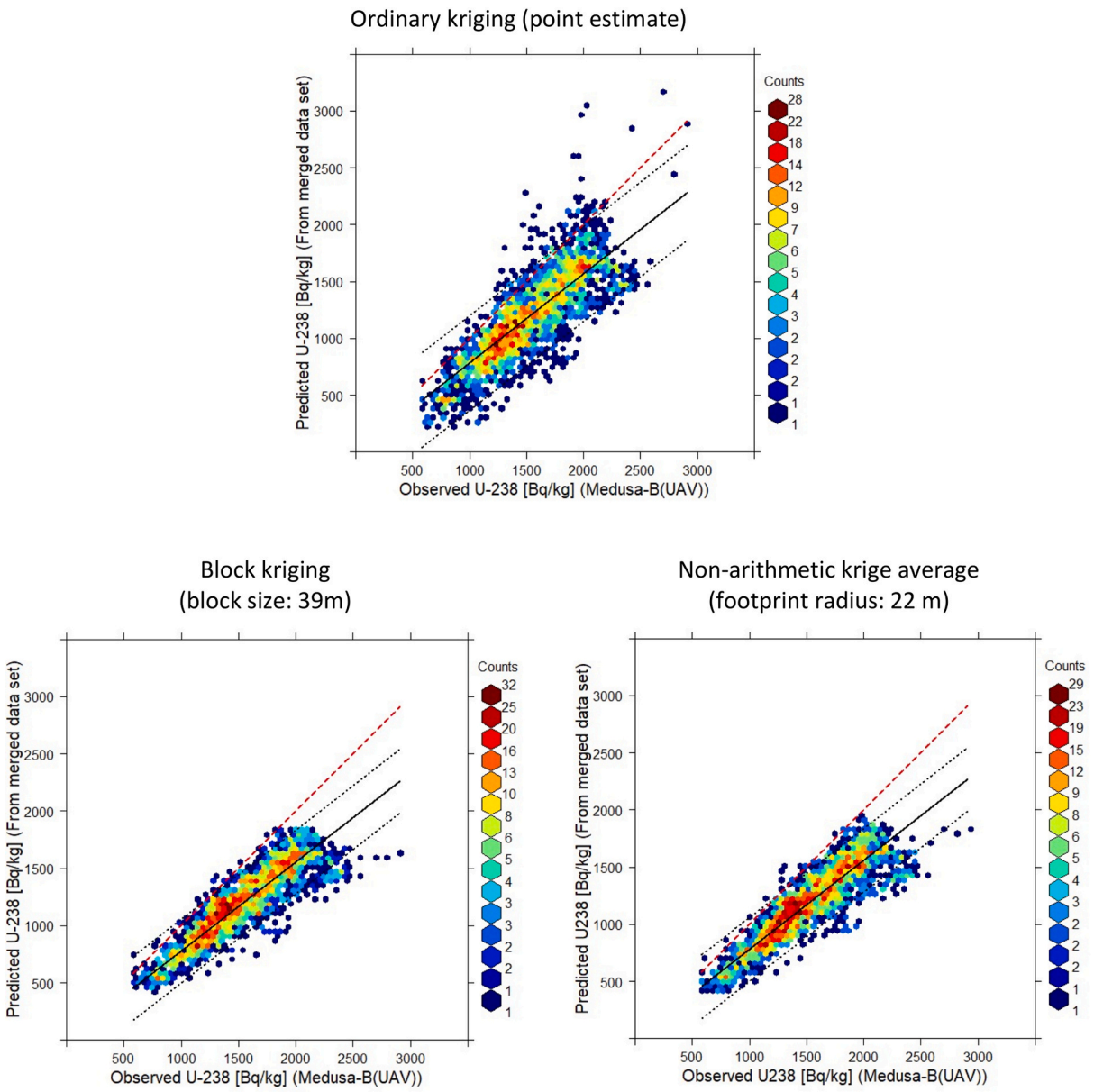

Fig. 7. Scatter plots of observed vs. predicted Medusa-B UAV U-238 specific activities. Variogram estimation and kriging interpolation was done with the merged backpack data set. Note that the data is binned in hexagonal bins. The color represents the number of data points within each bin. The dashed red line is the 1:1 line. The solid black line is the linear regression line forced through zero. The dashed black lines indicate the 95 % prediction band. From top to bottom the bias adjusted NSE is 0.51, 0.77 and 0.75. (For interpretation of the references to color in this figure legend, the reader is referred to the Web version of this article.)

observed bias could be either a systematic underestimation or a systematic overestimation. A comparison of the means and standard deviations of the three estimation approaches Table 7 with the statistics of the UAV data in Table 5 shows that block kriging and non-arithmetic krige averaging (after correction for bias) better reflect the reduced sampling variance due to the aerial spatial averaging effect than ordinary kriging.

In Fig. 8, we compare the spatial distribution pattern of the specific activities of U-238 interpolated using the merged backpack data in combination with the three kriging methods described above with the ordinary-kriging interpolation of the original UAV data using the modelled semivariogram from Fig. 6. For this qualitative comparison, we choose an area delineated by the contours of the survey area overflown by the UAV, including a buffer of 10 m.

From left to right and top to bottom, Fig. 8 shows the respective interpolation of the merged backpack specific activities of U-238 by 1)

Table 7
Number of predictions n, mean m, standard deviation σ (uncorrected and bias corrected in brackets) of the kriged estimates.

	Ordinary kriging	Block kriging	Non-arithmetic krige average
n	2840	2840	2840
m (m bias corrected)	1192 (1523)	1193 (1536)	1195 (1534)
σ (σ bias corrected)	380 (485)	307 (395)	316 (406)

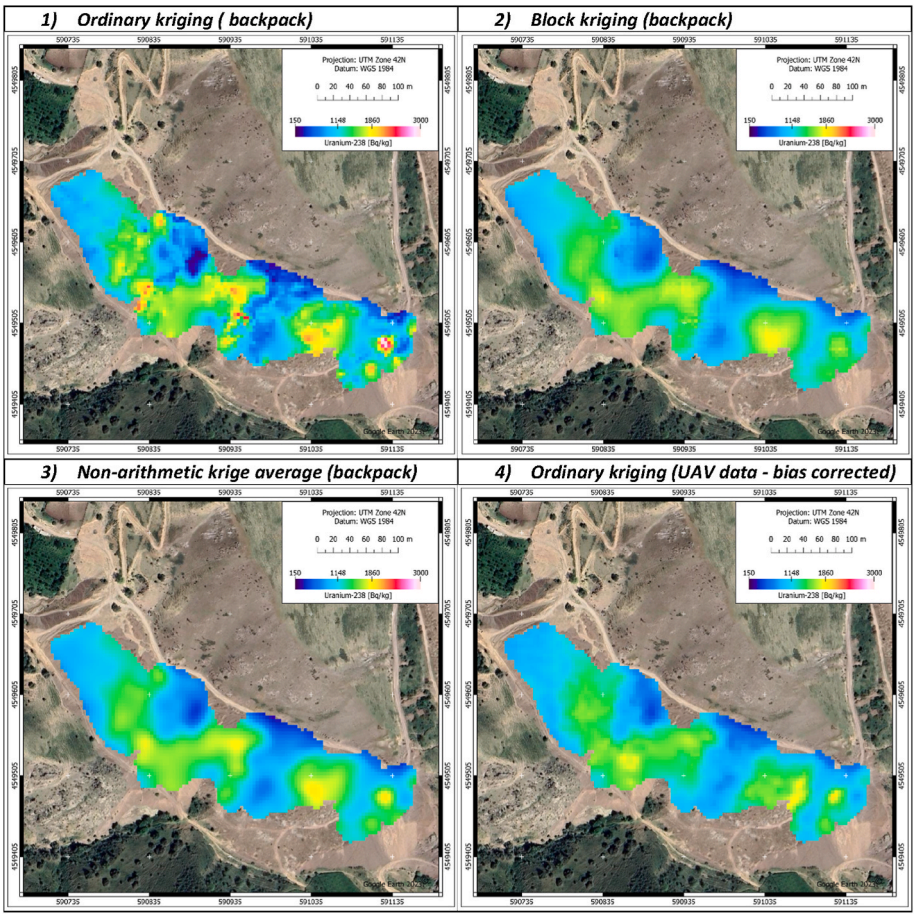

Fig. 8. Interpolation of the merged backpack specific activities of U-238 by 1) ordinary kriging, 2) block kriging and 3) non-arithmetic krige averaging to the total survey area of the UAV (enclosing polygon + 10 m buffer). Panel 4) shows the direct interpolation of the UAV measured specific activities of U-238 by ordinary kriging to the survey area. Note that the data in panel 4 is bias corrected by 22 %. (For interpretation of the references to color in this figure legend, the reader is referred to the Web version of this article.)

ordinary kriging, 2) block kriging, 3) non-arithmetic krige averaging and 4) direct interpolation of the UAV measured specific activities of U-238 by ordinary kriging to the survey area. The latter interpolation was done with the 22 % bias-corrected data as discussed above.

The basic pattern of the spatial distribution of the specific activities of U-238 agrees satisfactorily in all four panels of Fig. 8. As expected, the ordinary kriging interpolation map of the merged backpack data in panel 1 shows the greatest detail due to the detector measurement height of 1 m and the resulting high resolution. Compared to the ordinary kriging interpolation map of the UAV-measured data in panel 4, the agreement is good, but not as good as the interpolation results of the other two methods in panels 2 and 3, both of which track the spatial averaging of specific activities of U-238 by the UAV-based detector when interpolating the merged backpack data.

Comparing panels 2 and 3 with panel 4, it can be seen that the non-arithmetic krige averaging map in panel 3 captures details of the UAV measurement data (such as hotspots) slightly better than the block kriging map in panel 2, suggesting that the non-arithmetic averaging process represents the UAV data better than the block kriging approach.

Both upscaling approaches (panel 2 and 3) model the "shift to the mean" effect described by van der Veeke et al. (2021b) quite well. The effect describes the tendency of UAV-measurements to shift (on average) toward the mean of the overall distribution of the data, which is due to the greater spatial aggregation that occurs with increasing UAV altitude as the footprint becomes larger. The effect describes the tendency of the UAV measurements to shift (on average) towards the mean value of the overall distribution of the data, which is due to the stronger spatial aggregation that occurs with increasing UAV altitude as the footprint increases. Irrespective of this "average" development in spatial aggregation, individual values in the peripheral areas of hot spots can also be overestimated locally without, however, coming anywhere near the local extreme values of the hot spots. As with the UAV measurements in panel 4, the concentration peaks and troughs in panels 2 and 3 in Fig. 8 are attenuated and “shifted to the mean”. By scaling the backpack measurements to the footprint of the UAV, the effect is predicted in both upscaling approaches.

In Fig. 9 the spatial distributions of the residuals of the three scatter plots in Fig. 7 are shown. Fig. 9 shows residuals calculated by subtracting the predictions based on the merged backpack data (using the three different kriging approaches) from the Medusa-B data measured along the UAV flight path. The residuals are shown as relative residuals in % of the UAV Medusa-B measurement.

As discussed above we corrected the UAV Medusa-B data for the observed 22 % bias before calculating the residuals. The spatial distributions of observed versus predicted specific activities of U-238 as estimated with the three different kriging approaches described above show a decreasing range of the relative residuals with −96 to 70 % for ordinary kriging, −61 to 42 % for block kriging and −57 to 42 % for non-arithmetic krige averaging. As already discussed in the comparison of the scatter plots shown in Fig. 7, the explicit consideration of the distance dependency in the geostatistical modelling of the total signal measured with the UAV leads to the smallest positive and negative residuals in terms of magnitude. Fig. 9 also shows that for block kriging and non-arithmetic krige averaging, the areas where the UAV detector

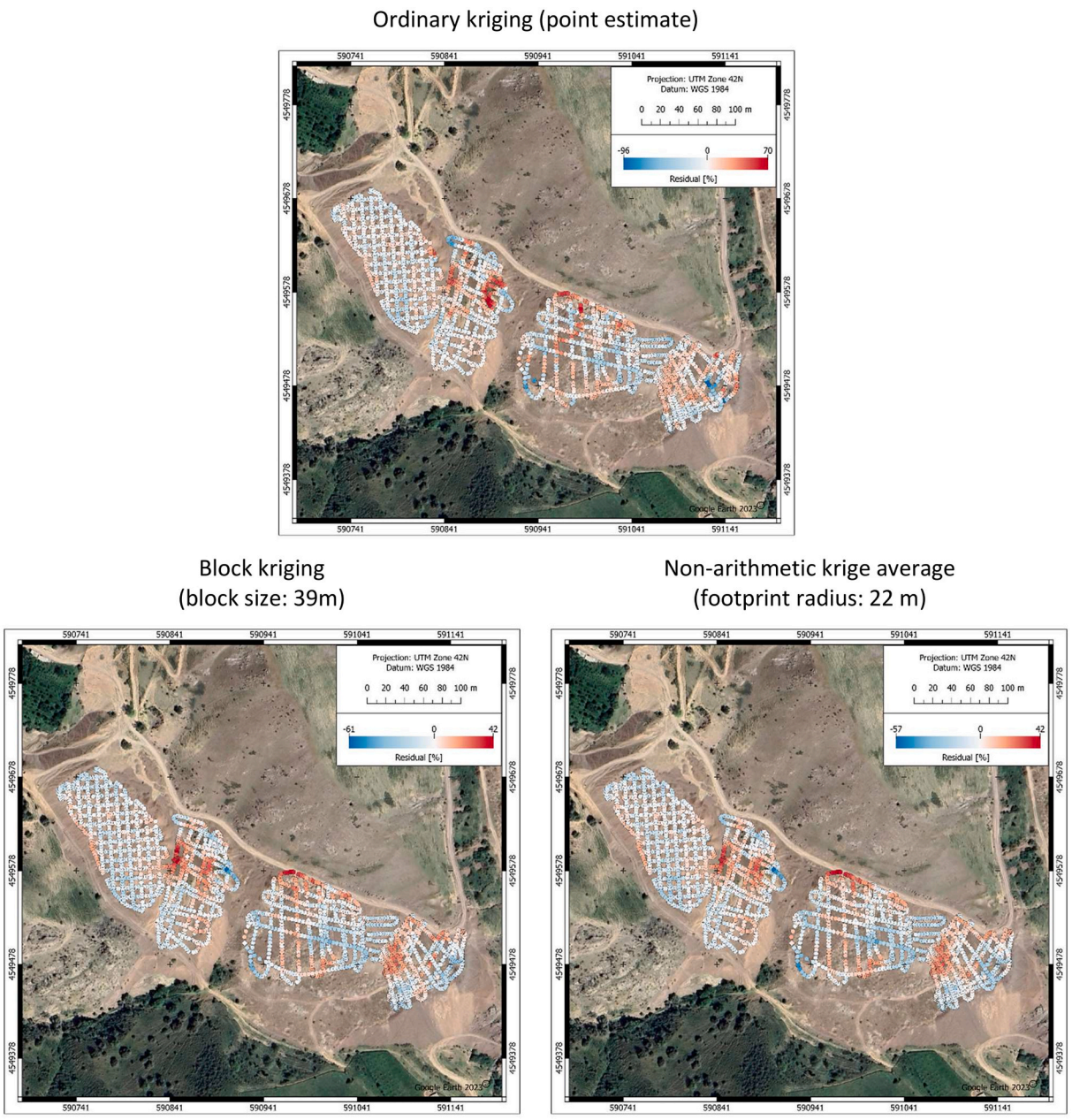

Fig. 9. Spatial distributions of the relative residuals (interpolated and/or upscaled backpack data minus the bias corrected UAV-Medusa-B measurements) of the three scatter plots shown in Fig. 7. The relative residuals are given in % of the Medusa B measurement. (For interpretation of the references to color in this figure legend, the reader is referred to the Web version of this article.)

signal is greatly overestimated or underestimated are small compared to the areas where prediction and measurement agree quite well. It seems that these areas are where the gradients of the measured gamma signal are quite steep (see Fig. 8).

Since the residuals shown in Fig. 9 are calculated from the bias corrected activities measured with Medusa-B along the UAV flight path and the interpolated activities from the merged backpack data set for the respective UAV measurement points, the residuals are at least partially determined by interpolation error. Both ordinary kriging and block kriging, as shown in Fig. 9, have the advantage over non-arithmetic kriging averaging that they additionally quantify interpolation uncertainty by calculating a local kriging variance in addition to the kriging estimate, thus enabling the interpolation error to be analysed in principle.

The assumption that the kriging variance is a measure of the uncertainty of the kriging interpolation is controversial and has both supporters (Heuvelink and Pebesma, 2002) and opponents (Journel 1993; Goovaerts, 1997). A simple check to quantify the influence of the interpolation error on the residuals is to plot the absolute residuals calculated for Fig. 9 against the square root of the local kriging variance (the kriging standard error) at the interpolated locations. Although one would not expect a strong relationship one should see an increasing absolute residual with increasing kriging standard error (Isaaks and Srivastava, 1989).

For ordinary kriging, Fig. 10 shows no positive correlation between the two variables, while there is a weak positive correlation for block kriging (correlation coefficent r of 0.22). The range of the modelled kriging standard errors at their lower end is limited by the estimated nugget variance (its square root). The observation indicates that the remaining residuals in the discussed comparisons of the upscaled backpack data with the bias-corrected UAV data (Figs. 8 and 9) are most likely influenced by other (unknown) processes and only to a smaller

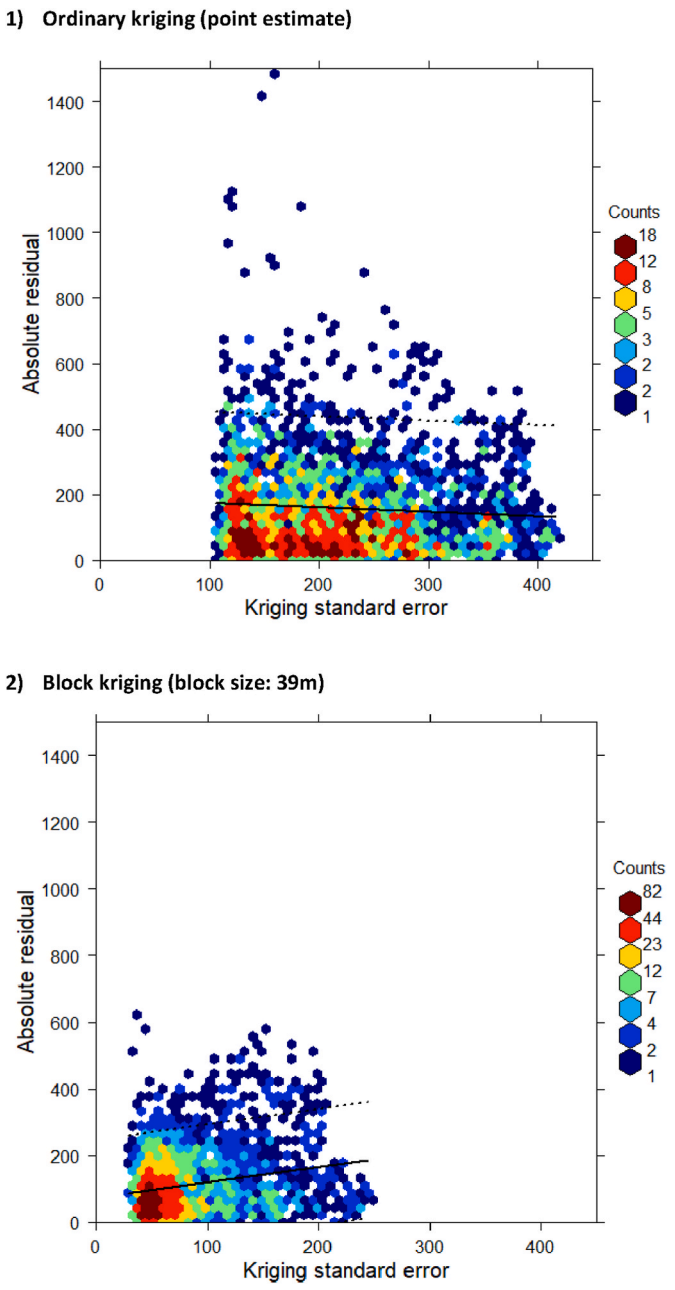

Fig. 10. Scatter plot of absolute residuals (interpolated and/or upscaled backpack U-238 activity data minus bias corrected UAV-Medusa-B measurements) vs. local kriging standard errors for 1) ordinary kriging and 2) block kriging. Note that the data is binned in hexagonal bins. The color represents the number of data points within each bin. The solid black line is the linear regression. The dashed black lines indicate the 95 % prediction band. (For interpretation of the references to color in this figure legend, the reader is referred to the Web version of this article.)

extent by interpolation error. These unknown processes could, for example, be gradient, geometry or edge effects due to differences in the geometry of the backpack and UAV-based gamma spectrometry.

After a linear regression with intercept, as shown in Fig. 10, no part of the variance of the residuals can be explained by the standard error calculated with ordinary kriging and only 5 % by the standard error of block kriging. From this it may be concluded that in ordinary kriging (due to the obvious scale incompatibility) the kriging standard error is not a predictor for the variance of the residuals, whereas in block kriging 5 % of the variance of the residuals is related to interpolation errors.

6. Conclusion

We have shown that geostatistics is a valuable tool for quantitative comparison of UAV-based GRS with backpack GRS across the scale differences arising from different detector altitudes of the two systems. It allows to account for the change in spatial support associated with the transition from backpack to UAV-based measurements and is useful for cross-checking the various techniques used in GRS to correct for flight altitude and other influencing variables when converting radionuclide specific counts to activity concentrations of the soil.

The two interpolation techniques applied here to upscale the specific U-238 activities measured by two backpack GRS systems, ordinary block kriging and the slightly more complicated non-arithmetic Krige averaging, perform very similarly in predicting the specific U-238 activity distribution measured by a UAV-GRS system over the surface of an extensive low-grade uranium mine dump in Uzbekistan. They capture the characteristics of the spatial distribution of specific U-238 activities and their statistical distribution properties much better than ordinary kriging, which lacks such upscaling properties.

Further studies at different sites and with different distributions of specific activities are needed to either confirm these results or provide new insights.

Funding

The study was funded by the German Federal Ministry of Education and Research (BMBF) under the CLIENT II program, Grant No. 01LZ1706A-D. The International Atomic Energy Agency's (IAEA) Coordination Group for Uranium Legacy Sites (CGULS) program has facilitated participation of Central Asian experts in practical workshops and coordination meetings and provided logistical assistance for the field work. CGULS also provided support to practical training of Central Asian experts during the field tests described in this paper.

CRediT authorship contribution statement

Sven Altfelder: Writing – review & editing, Writing – original draft, Project administration, Methodology, Funding acquisition, Conceptualization. **Benedikt Preugschat:** Visualization, Software, Project administration, Investigation, Conceptualization. **Milan Matos:** Investigation, Formal analysis. **Felix Kandzia:** Software, Investigation, Formal analysis. **Benjamin Wiens:** Investigation, Conceptualization. **Otabek Eshmuradov:** Resources, Investigation. **Christian Kunze:** Project administration, Formal analysis, Conceptualization.

Declaration of competing interest

The authors declare the following financial interests/personal relationships which may be considered as potential competing interests: The authors declare no conflict of interest. The funders had no role in the design of the study; in the collection, analyses, or interpretation of data; in the writing of the manuscript, or in the decision to publish the results.

Sven Altfelder reports financial support was provided by German Federal Ministry of Education and Research (BMBF). Sven Altfelder reports financial support was provided by International Atomic Energy Agency Department of Nuclear Safety and Security.

Data availability

Data will be made available on request.

References

Ammar, A.A., 1996. Characteristic aerial and ground radioactives of basement and sedimentary rocks in Egypt: relations and natural cycles across geologic time. In: Proceedings of the Third Arab Conference on the Peaceful Uses of Atomic Energy. Dec, pp. 9–13. Damascus.

Bollhöfer, A., Pfitzner, K., Ryan, B., Fawcett, M., 2007. Ground Truthing of an Airborne Gamma Survey and Assessment of the Radiological Conditions of the Sleisbeck Mine Area, Internal Report 526. Department of the Environment and Heritage, Australia.

Bollhöfer, A., Beraldo, A., Pfitzner, K., Esparon, A., Doering, C., 2014. Determining a pre-mining radiological baseline from historic airborne gamma surveys: a case study. Sci. Total Environ. 468, 764–773. https://doi.org/10.1016/j.scitotenv.2013.09.001. –469.

Buchanan, E., Cresswell, A.J., Seitz, B., Sanderson, D.C.W., 2016. Operator related attenuation effects in radiometric surveys. Radiat. Meas. 86, 24–31.

Burrough, P.A., McDonnell, R.A., Lloyd, C.D., 2015. Principles of Geographical Information Systems. Oxford university press.

Duval, J.S., Cook, B., Adams, J.A.S., 1971. Circle of investigation of an air-borne gamma ray spectrometer. J. Geophys. Res. 76 https://doi.org/10.1002/bse.1893. December.

EU, 2019a. Commission Delegated Regulation (EU) 2019/945 of 12 March 2019 on Unmanned Aircraft Systems and on Third-Country Operators of Unmanned Aircraft Systems OJ L 152/1. Available online: https://eur-lex.europa.eu/legal-content/EN/TXT/?uri=CELEX%3A32019R0945. (Accessed 18 July 2023).

EU, 2019b. Commission Implementing Regulation (EU) 2019/947 of 24 May 2019 on the Rules and Procedures for the Operation of Unmanned Aircraft OJ L 152/45. Available online: https://eur-lex.europa.eu/legal-content/EN/TXT/?uri=CELEX%3A32019R0947. (Accessed 18 July 2023).

Goovaerts, P., 1997. Geostatistics for Natural Resources Evaluation. Oxford Univ. Press, New York.

Goovaerts, P., 1999. Geostatistical tools for deriving block-averaged values of environmental attributes. J. Geographical Information Sci. 5, 88–96.

Grasty, R.L., Kosanke, K.L., Foote, R.S., 1979. Fields of view of airborne gamma-ray detectors. Geophysics. https://doi.org/10.1190/1.1441017.

Grasty, R., Minty, B., 1995. A Guide to the Technical Specifications for Airborne Gamma-Ray Surveys. Australian Geological Survey Organisation. Record 1995/60.

Heuvelink, G., Pebesma, E., 2002. Is the ordinary kriging variance a proper measure of interpolation error?. In: Spatial Accuracy Conference Melbourne. https://www.researchgate.net/publication/46629588_Is_the_ordinary_kriging_variance_a_proper_measure_of_interpolation_error.

IAEA, 2003. Guidelines for Radioelement Mapping Using Gamma Ray Spectrometry Data; TECDOC 1363. International Atomic Energy Agency, Vienna, Austria.

Isaaks, E.H., Srivastava, R.M., 1989. An Introduction to Applied Geostatistics. Oxford Univ. Press, New York.

Journel, A.G., 1993. Geostatistics: roadblocks and challenges. In: Soares, A. (Ed.), Geostatistics Troia '92. Kluwer Academic Publishers, Dordrecht, pp. 213–224.

Kock, P., Samuelsson, C., 2011. Comparison of airborne and terrestrial gamma-ray spectrometry measurements - evaluation of three areas in Southern Sweden. J. Environ. Radioact. 102, 605–613.

Kunze, C., Preugschat, B., Arndt, R., Kandzia, F., Wiens, B., Altfelder, S., 2022. Development of a UAV-based gamma spectrometry system for natural radionuclides and field tests at central Asian uranium legacy sites. Rem. Sens. 14, 2147. https://doi.org/10.3390/rs14092147.

MacFarlane, J.W., Payton, O.D., Keatley, A.C., Scott, G.P.T., Pullin, H., Crane, R.A., Smilion, M., Popescu, I., Curlea, V., Scott, T.B., 2014. Lightweight aerial vehicles for monitoring, assessment and mapping of radiation anomalies. J. Environ. Radioact. https://doi.org/10.1016/j.jenvrad.2014.05.008.

Martin, P.G., Payton, O.D., Fardoulis, J.S., Richards, D.A., Scott, T.B., 2015. The use of unmanned aerial systems for the mapping of legacy uranium mines. J. Environ. Radioact. https://doi.org/10.1016/j.jenvrad.2015.02.004.

Martin, P.G., Payton, O.D., Fardoulis, J.S., Richards, D.A., Yamashiki, Y., Scott, T.B., 2016. Low altitude unmanned aerial vehicle for characterising remediation effectiveness following the FDNPP accident. J. Environ. Radioact. 151 https://doi.org/10.1016/j.jenvrad.2015.09.007.

Matheron, G., 1963. Principles of geostatistics. Econ. Geol. 58, 1246–1266.

Minty, B., 1997. Fundamentals of airborne gamma-ray spectrometry, AGSO. Journal of Australian Geology and Geophysics 17 (2), 39–50.

Neuweiler, I., Vogel, H.J., 2007. Upscaling for unsaturated flow for non-Gaussian heterogeneous porous media. Water Resour. Res. 43 (3).

Nicolet, J.P., Erdi-Krausz, G., 2003. Guidelines for Radioelement Mapping Using Gamma Ray Spectrometry Data, vol. 179. International Atomic Energy Agency. http://www-pub.iaea.org/MTCD/publications/PDF/te_1363_web.pdf.

Ogunsanwo, F.O., Olurin, O.T., Ogunsanwo, B.T., Okeyode, I.C., Olowofela, J.A., 2019. Correlations between airborne and terrestrial gamma-ray spectrometric data in the bitumen deposit area, Ogun State, Nigeria. Scientific African 5, e00133. https://doi.org/10.1016/j.sciaf.2019.e00133.

Oliver, M.A., Webster, R., 2014. A tutorial guide to geostatistics: computing and modelling variograms and kriging. Catena 113 (1), 56–69.

Pebesma, E.J., 2004. Multivariable geostatistics in S: the gstat package. Comput. Geosci. 30, 9.

Pebesma, E., Graeler, B., Pebesma, M.E., 2015. Package 'gstat'. Comprehensive R Archive Network (CRAN), p. 1, 0.

Pirttijärvi, M., Oy, R., 2016. Radai's UAV based radiometric measurements at Rautuvaara mine in Kolari. Radai Survey Report. www.radai.fi.

Preugschat, B., Kunze, C., Arndt, R., Kandzia, F., Wiens, B., Altfelder, S., 2022. Drone-based Gamma Spectrometry of NORM-Affected Areas and Uranium Legacy Sites: Results and Outlook of the DUB-GEM Research & Development Project. NORM X Utrecht, Netherlands, pp. 9–13. May (to appear as IAEA publication).

R Core Team, 2021. R: A Language and Environment for Statistical Computing. R Foundation for Statistical Computing, Vienna, Austria. URL. https://www.R-project.org/.

Ridikas, D., Darby, I.G., Kaiser, R., Maekawa, A., Matos, M., Saito, H., Sladek, P., Bogovac, M., 2023. Rapid environmental mapping with Instrumented unmanned aerial vehicle: experience and lessons learned from the commissioning and trial measurements in the areas affected by TEPCO fukushima daiichi nuclear power plant accident. Nucl. Phys. News 33 (2), 22–27.

Tyler, A.N., 1994. Environmental influences on gamma ray spectrometry. PhD Thesis. Glasgow University.

van der Veeke, S.L.J., Koomans, R.L., Söderström, M., de Waal, S.N., van der Graaf, E.R., 2021a. Footprint and height corrections for UAV-borne gamma-ray spectrometry studies. J. Environ. Radioact. 231.

van der Veeke, S.L.J., Koomans, R.L., Söderström, M., van der Graaf, E.R., 2021b. Optimizing gamma-ray spectrometers for UAV-borne surveys with geophysical applications. J. Environ. Radioact. 237.

van der Veeke, S., 2023. UAV-Borne Radioelement Mapping: towards a Guideline and Verification Methods for Geophysical Field Measurements. [Thesis fully internal (DIV), University of Groningen]. University of Groningen. https://doi.org/10.33612/diss.261264637.

Webster, R., Oliver, M., 2001. Geostatistics for Environmental Scientists Statistics in Practice. Wiley, Chichester, p. 271.

Youssef, M.A.S., 2016. Relationships between ground and airborne gamma-ray spectrometric survey data, north Ras Millan, southern Sinai Peninsula, Egypt. J. Environ. Radioact. 152, 75–84.